High-frequency electron spin resonance in magnetic systems

2000 J. Phys.: Condens. Matter 12 R589

(http://iopscience.iop.org/0953-8984/12/47/201)

J. Phys.: Condens. Matter **12** (2000) R589–R614. Printed in the UK PII: S0953-8984(00)78683-8

TOPICAL REVIEW

High-frequency electron spin resonance in magnetic systems

Koichi Katsumata

RIKEN (The Institute of Physical and Chemical Research), Wako, Saitama 351-0198, Japan
and
RIKEN Harima Institute, Mikazuki, Sayo, Hyogo 679-5148, Japan

Received 5 September 2000, in final form 25 October 2000

Abstract. We review the recent progress in the study of magnetic materials using a high-frequency electron spin-resonance (ESR) technique. First, we show how useful high-frequency ESR is for studying antiferromagnetic materials, where the ESR frequency and magnetic field depend greatly on the exchange interaction and anisotropy energy of the materials. Next, we review the recent high-frequency ESR experiments made on spin $S = 1$ quasi-one-dimensional Heisenberg antiferromagnets (Q1D HAFs) and the spin–Peierls system $CuGeO_3$. Then, we review the ESR studies performed on more complex systems, such as an $S = 1$ Q1D HAF with bond alternation, spin-ladder compounds and quasi-two-dimensional magnets. Each of these systems has a singlet ground state of quantum origin and an energy gap to the lowest excited state. On applying an external magnetic field, these systems show a transition from the non-magnetic to a magnetized state, and in some cases, long-range magnetic ordering occurs. Efforts are made to explain the underlying physics intuitively at the expense of rigour.

1. Introduction

The phenomenon of electron spin resonance (ESR) was discovered in 1945 by Zavoisky [1]. At about the same time that of nuclear magnetic resonance (NMR) was also discovered [2, 3]. These magnetic resonance techniques have been used to elucidate many interesting properties of materials from a microscopic point of view.

The basic principle of ESR is as follows. The magnetic properties of matter originate, in most cases, from the spin and orbital moments of electrons. When a paramagnetic material is immersed in a magnetic field, $\boldsymbol{B}$, a magnetization, $\boldsymbol{M}$, is induced by $\boldsymbol{B}$†.

Since $\boldsymbol{M}$ is proportional to the angular momenta, we have the following equation of motion:

$$\mathrm{d}\boldsymbol{M}/\mathrm{d}t = \gamma[\boldsymbol{M} \times \boldsymbol{B}]. \tag{1}$$

The stationary solution of equation (1) gives a precession of $\boldsymbol{M}$ around $\boldsymbol{B}$ whose frequency, ν, is given by

$$\nu = \gamma B/2\pi. \tag{2}$$

If a microwave with frequency ν is fed perpendicularly to $\boldsymbol{B}$, i.e., in the plane of the precession, the energy of the microwave is absorbed by the magnetic system. The energy absorbed by the magnetic system then flows to the heat reservoir. Because of this, we are able to observe the absorption of the microwaves by magnetic materials.

† It is noted that $\boldsymbol{H}$ has been widely used as the notation for a magnetic field. In the following, we use $\boldsymbol{B}$ to represent a magnetic field except in the figures which have been taken from the literature. For consistency with the figures, we sometimes use $\boldsymbol{H}$ in parallel to $\boldsymbol{B}$ in the text.

0953-8984/00/470589+26$30.00

For the quantum mechanical description of the ESR phenomena, we consider the simplest case in which non-interacting magnetic atoms exist in the sample, each of which has a magnetic moment $g\mu_B \boldsymbol{S}$, where g is the g-value, μ_B the Bohr magneton and $\boldsymbol{S}$ the spin operator. In applied magnetic fields, each magnetic atom shows $2S + 1$ Zeeman split levels with energies $g\mu_B S_z B$, where S_z $(=S, S-1, \ldots, -S)$ is the z-component of $\boldsymbol{S}$ $(\boldsymbol{z} \parallel \boldsymbol{B})$. If an oscillating magnetic field $\boldsymbol{b}\cos(2\pi\nu t)$ is applied perpendicularly to $\boldsymbol{B}$, say along the x-direction, this oscillating field induces transitions between the energy levels whose S_z-values differ by ± 1. This is due to the fact that the matrix element bS_x, which is proportional to the transition probability, has a non-zero value when connecting states whose S_z-values differ by ± 1. From a simple calculation, we have the relation $h\nu = g\mu_B B$, which is the same as that obtained from the classical equation of motion, equation (1), if we set $\gamma = 2\pi g\mu_B/h$ in equation (2), where h is Planck's constant.

The relation between the energy and momentum of electromagnetic waves (light) is much steeper than that of magnetic systems; one measures the excitation spectrum only at zero momentum by means of ESR. This is a disadvantage of the ESR technique in studying condensed matter compared with neutron scattering methods which can probe a wide range of momentum space. The advantages of ESR methods over others include the high sensitivity and high energy resolution.

The term ESR has been widely used to describe magnetic resonance phenomena where electron spins play an essential role. Chemists and biologists have been using the term 'electron paramagnetic resonance (EPR)' because the samples that they are interested in have mostly been paramagnetic [4]. Since the resonant frequency of EPR is proportional to the resonant magnetic field as can be seen from equation (2), one might say that one does not need high-frequency–high-field ESR apparatus. As science advances, researchers handle more complex systems in which EPR signals become overlapped. The same is true for NMR. In such cases, we can resolve the signals by increasing the frequency and consequently the magnetic field. This is why the frequency of a high-resolution NMR spectrometer continues to increase. There has also been progress in the development of a high-frequency–high-field EPR spectrometer for chemical research [5].

In this article, we review the recent achievements made in the field of magnetism using a high-frequency–high-field ESR technique. Here, we use the term 'high' frequency rather broadly. The most popular ESR spectrometer commercially available operates in the X band (where $\nu \sim 10$ GHz). The highest-frequency machine now commercially available works at $\nu \sim 90$ GHz. So, ESR measurements made above $\sim$100 GHz may be considered as at 'high' frequency. Although the development of the technique is essential in this field of research, we will not describe the technique here, because this may not be interesting to the readers of this journal. We will try to explain the physics obtained from these studies, rather than present a collection of data.

In section 2, we show the result of an ESR measurement made on an antiferromagnet which demonstrates that high-frequency ESR is indispensable for obtaining information on the magnetic properties. We call ESR in the antiferromagnetically ordered phase 'antiferromagnetic resonance (AFMR)' [6]. ESR in the ordered phase of a ferromagnet is called 'ferromagnetic resonance (FMR)'. The relation between the resonant frequency and magnetic field of FMR is determined from equation (1) by replacing $\boldsymbol{B}$ with the internal field, $\boldsymbol{B} - N\boldsymbol{M}$, where N is the demagnetizing factor of the sample.

In recent years, quantum effects in lower-dimensional magnets have been attracting great interest. After summarizing basic knowledge about lower-dimensional magnetism in section 3, we review the ESR studies on these quantum magnets in section 4. In section 5 we review some ESR results obtained for more complex systems.

2. Antiferromagnetic resonance

The transition metal difluorides, MF_2 (M = Mn, Fe, Co), are a typical example of insulating antiferromagnets [7]. Figure 1 shows the crystal and magnetic structures of MnF_2. This compound exhibits an antiferromagnetic ordering below 67.3 K with the spin easy axis parallel to the c-axis.

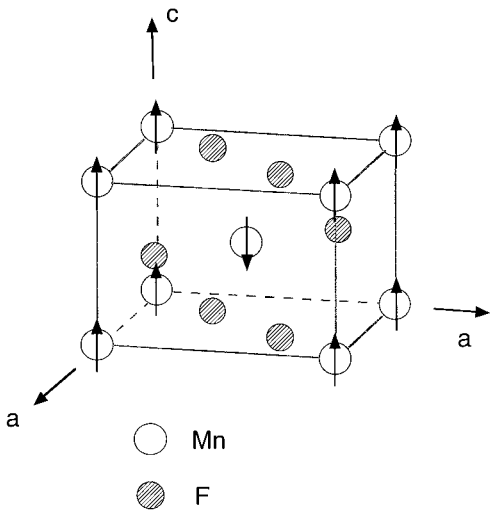

Figure 1. The crystal and magnetic structures of MnF_2. Arrows show the magnetic moment.

Figure 2 shows the results of AFMR measurements made on a single crystal of MnF_2 at low temperatures well below the ordering temperature [8,9]. Even at $B = 0$, we have a finite ESR frequency at 259.7 GHz. On applying $\boldsymbol{B}$ parallel to the c-axis, we observe two branches, for one of which the ESR frequency increases with increasing field, while it decreases with field and becomes zero at 9.3 T for the other branch. Above 9.3 T, we have a single branch whose ESR frequency increases with increasing field. When $\boldsymbol{B}$ is applied perpendicularly to the c-axis, we see a single branch with a finite frequency at $B = 0$.

Let us consider what is happening at 9.3 T. Figure 3 shows the temperature dependence of the magnetic susceptibility, χ, of MnF_2 [8] whose form is typical of a uniaxial antiferromagnet. Below the antiferromagnetic ordering temperature, T_N, χ along the spin easy axis, $\chi_\parallel$, decreases with decreasing temperature, because the magnetic moments order as shown in figure 1 where the net magnetization decreases to zero with decreasing temperature. If we turn the magnetic moments perpendicular to the easy axis along which $\boldsymbol{B}$ is applied, a net magnetization is induced along $\boldsymbol{B}$, the rate of which does not depend much on temperature as is evident from the behaviour of $\chi_\perp$ in figure 3. Strictly speaking, $\chi_\perp$ shown in figure 3 is the susceptibility when $\boldsymbol{B}$ is applied perpendicularly to the c-axis. However, $\chi_\perp(\boldsymbol{B} \parallel \boldsymbol{c})$ is almost the same as $\chi_\perp(\boldsymbol{B} \perp \boldsymbol{c})$. Therefore, we expect a flopping of the magnetic moments to occur at the critical field denoted by B_{SF}, where the gain in the magnetic energy exceeds the loss in the anisotropy energy.

A theoretical treatment of AFMR has been successfully carried out on the basis of a two-sublattice model with a molecular-field approximation [10]. The up sublattice, $\boldsymbol{M}^+$, represents all of the magnetic moments that point upwards and the down sublattice, $\boldsymbol{M}^-$, all of those pointing downwards. We introduce an exchange field, $\boldsymbol{B}_E$, originating from the

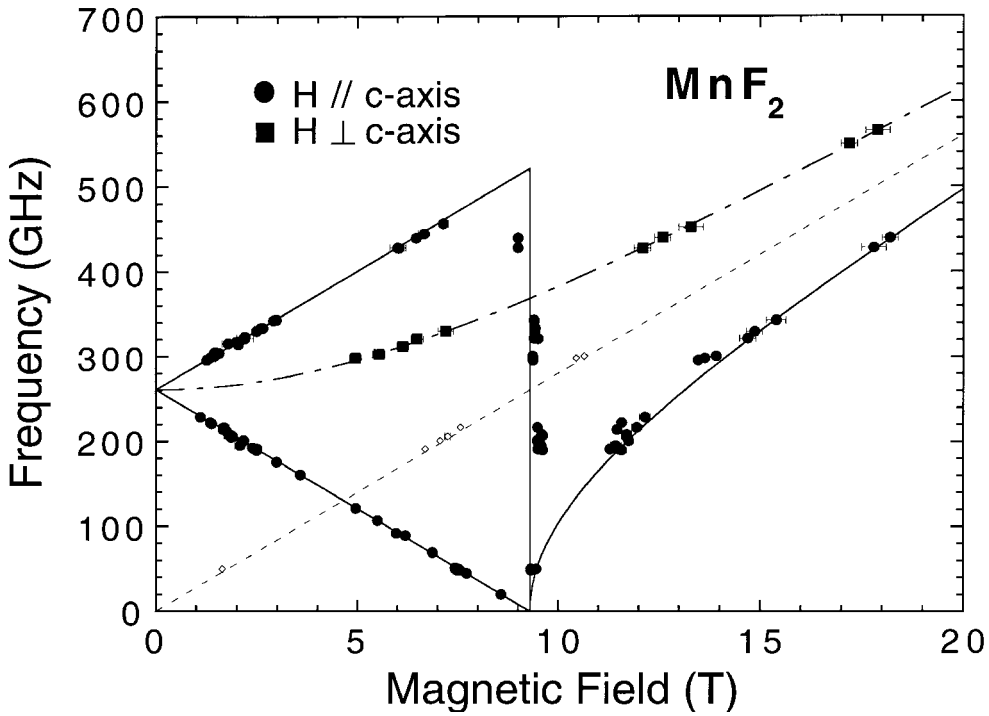

Figure 2. The frequency versus magnetic field plot of the ESR signals observed in a single-crystal sample of MnF_2 in the antiferromagnetically ordered phase. (Figure from reference [9].)

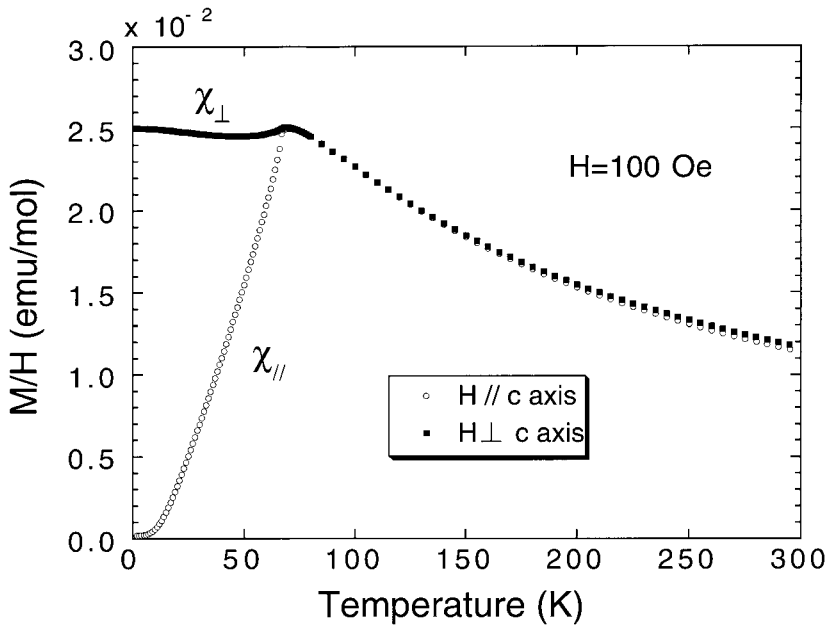

Figure 3. The temperature dependence of the magnetic susceptibility of MnF_2 parallel and perpendicular to the *c*-axis. (Figure from reference [8].)

exchange interaction between spins. We also introduce an anisotropy field, $\boldsymbol{B}_{\mathrm{A}}$, which forces the magnetic moments to point parallel or antiparallel to the spin easy axis (the c-axis in MnF_2). Then, we have the equation of motion for each of $\boldsymbol{M}^+$ and $\boldsymbol{M}^-$ in the form given by equation (1) with $\boldsymbol{B}$ replaced by $\boldsymbol{B}+\boldsymbol{B}_{\mathrm{E}}+\boldsymbol{B}_{\mathrm{A}}$. After a simple calculation we have, in the case of $\boldsymbol{B} \parallel c$-axis,

$$h\nu/g\mu_{\mathrm{B}} = \sqrt{2K_{\mathrm{u}}/\chi_{\perp} + (\chi_{\parallel}B/2\chi_{\perp})^2} \pm B(1 - \chi_{\parallel}/2\chi_{\perp}) \tag{3}$$

for $B < B_{\mathrm{SF}}$ and

$$h\nu/g\mu_{\mathrm{B}} = \sqrt{B^2 - 2K_{\mathrm{u}}/\chi_{\perp}} \tag{4}$$

for $B > B_{\mathrm{SF}}$. Here, we have used the relations $B_{\mathrm{E}} = M_0/\chi_{\perp}$ and $B_{\mathrm{A}} = K_{\mathrm{u}}/M_0$, where M_0 is the magnitude of the sublattice magnetization at $T = 0$ and K_{u} is the anisotropy constant. At low temperatures, $\chi_{\parallel}$ is much smaller than $\chi_{\perp}$ and so equation (3) becomes

$$h\nu/g\mu_{\mathrm{B}} = \sqrt{2K_{\mathrm{u}}/\chi_{\perp}} \pm B. \tag{5}$$

Equation (5) represents the two branches in figure 2 below 9.3 T, while equation (4) represents the single branch above 9.3 T. When $\boldsymbol{B}$ is applied perpendicularly to the spin easy axis, we have

$$h\nu/g\mu_{\mathrm{B}} = \sqrt{B^2 + 2K_{\mathrm{u}}/\chi_{\perp}} \tag{6}$$

which represents the branch for $\boldsymbol{B} \perp c$-axis in figure 2.

The full and dash–dotted lines in figure 2 are theoretical ones, equations (4)–(6). If we adjust the two parameters, $\sqrt{2K_{\mathrm{u}}/\chi_{\perp}} = 9.27$ T and $g = 2.00$, the theory explains all of the experimental data quite well. The dotted line shows an EPR line with $g = 2.00$ along which a weak ESR signal is observed even in the ordered phase. The possibility of observing an EPR signal in the magnetically ordered phase has been predicted theoretically [11]. The vertical straight line at 9.3 T represents the critical field resonance mode [10] from which a weak ESR signal is observed.

The AFMR positions change with temperature. Figure 4 shows the temperature dependence of the resonance field of the AFMR mode given by equation (3) with the minus sign at fixed frequencies. In equation (3), K_{u}, $\chi_{\parallel}$ and $\chi_{\perp}$ depend on temperature. We use for the temperature dependence of the ratio $\chi_{\parallel}/\chi_{\perp}$ the experimental value deduced from figure 3. Then, we have only one adjustable parameter, $K_{\mathrm{u}}/\chi_{\perp}$. We obtain the temperature dependence of $K_{\mathrm{u}}/\chi_{\perp}$ by fitting equation (3) with the data taken at 50.5 GHz. We can then compare the theory with the experiments performed at 21.7 GHz and 36.8 GHz without any adjustable parameters. The agreement between theory and experiment at the two frequencies is satisfactory.

It may be recognized that an AFMR measurement gives important information on the magnetic properties, e.g., the exchange interaction, the anisotropy and the direction of the magnetic moments. The frequency at $B = 0$, $\sqrt{2K_{\mathrm{u}}/\chi_{\perp}}$, is given by the geometric mean of B_{E} and B_{A}. In order to study a wide variety of antiferromagnetic materials, one needs as wide a range of frequency and magnetic field as possible.

3. Fundamentals of lower-dimensional magnetism

In an insulating material, electrons are almost localized at the atomic sites with a small degree of covalent bonding to the neighbouring atoms. Therefore, we have a chance to fabricate a magnetic material in which the magnetic interaction in one direction dominates, with much weaker interactions in other directions. We define this class of materials as the quasi-one-dimensional (Q1D) magnets. Similarly, we define a quasi-two-dimensional (Q2D) magnet as

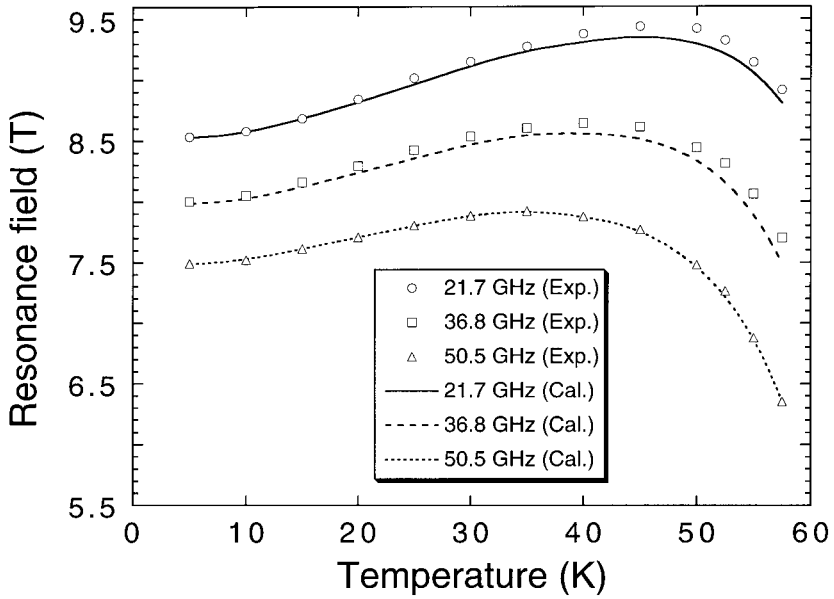

Figure 4. The temperature dependence of the resonance field in MnF_2 at the designated frequencies. The full and dashed curves are theoretical ones. (Figure from reference [8].)

one in which an overwhelming interaction exists in the plane with a much weaker interaction between planes. In insulating magnets a well defined magnetic moment exists at each atomic site. We denote this magnetic moment by $\boldsymbol{m}$ ($\equiv g\mu_B \boldsymbol{S}$) and call $\boldsymbol{S}$ the 'spin'. We include the effects of spin–orbit interaction and crystal fields in this definition, so the g-value deviates from its free-electron value 2.0023 and becomes anisotropic. The value of S can be $\frac{1}{2}$, 1, $\frac{3}{2}$, ... depending on the magnetic atom in question.

Because a 1D magnetic system is the simplest realization of interacting many-body problems, the study of 1D magnetism has a long history, starting with the pioneering work of Bethe [12]. In the 1960s and early 1970s, a number of real materials close to the model 1D and 2D systems were discovered [13], which greatly stimulated the development of the field. In the early 1980s, a new horizon was opened towards the understanding of quantum phenomena in lower-dimensional magnetic systems.

Let us start with the simplest case, shown in figure 5, in which two magnetic atoms with $S = \frac{1}{2}$ at sites 1 and 2 are coupled by an exchange interaction, J.

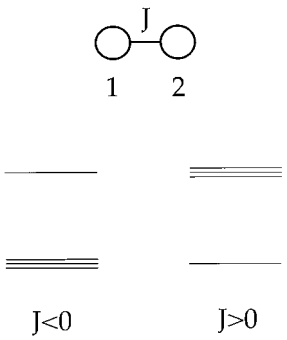

Figure 5. The energy level scheme for an exchange-coupled spin-$\frac{1}{2}$ dimer.

The Hamiltonian describing this system is given by

$$H = J\boldsymbol{S}_1 \cdot \boldsymbol{S}_2. \tag{7}$$

In the case of ferromagnetic interactions ($J < 0$), the ground state is a triplet with the eigenfunctions given by $\alpha(1)\alpha(2)$, $\beta(1)\beta(2)$ and $\{\alpha(1)\beta(2) + \beta(1)\alpha(2)\}/\sqrt{2}$, where $\alpha(1)$ and $\beta(2)$ are the eigenfunctions of $S_z = \frac{1}{2}$ at site 1 and $S_z = -\frac{1}{2}$ at site 2, respectively. The excited state is a singlet with the eigenfunction $\{\alpha(1)\beta(2) - \beta(1)\alpha(2)\}/\sqrt{2}$. The situation is reversed in the case of antiferromagnetic interactions ($J > 0$), as shown in figure 5.

Theoretical physicists have been studying purely 1D systems with the following Heisenberg Hamiltonian:

$$H = \sum_{i,j} J_{ij}\boldsymbol{S}_i \cdot \boldsymbol{S}_j \tag{8}$$

where J_{ij} is the exchange interaction between spins at sites i and j.

Figure 6(a) shows the simplest 1D magnetic model with the nearest-neighbour interaction only. In the case of ferromagnetic interactions, the situation is trivial. The ground state is the one with all of the magnetic moments aligned in one direction. On the other hand, in the case of antiferromagnetic interactions, the ground state is far from what we naïvely imagine. Anderson [14] pointed out that for an $S = \frac{1}{2}$ 1D Heisenberg antiferromagnet (HAF) the energy of a dimerized state, as depicted in figure 6(b), is lower than that of the classical Néel state, shown schematically in figure 6(c). The wave function (Ψ) of the dimerized state is given by

$$\Psi = (12)(34)(56)\cdots \tag{9}$$

where $(\cdot\cdot)$ represents the eigenfunction of the singlet state of equation (7) given above. It should be emphasized that the state given in figure 6(b) is a model which approximates the ground state of an $S = \frac{1}{2}$ 1D HAF better than the Néel state (figure 6(c)). The true ground state of the Hamiltonian (equation (8)) with $J_{ij} = J$ consists of all possible combinations of singlet dimers, called the resonating-valence-bond (RVB) ground state [14]. So, the ground state of an $S = \frac{1}{2}$ 1D HAF is a singlet of quantum origin.

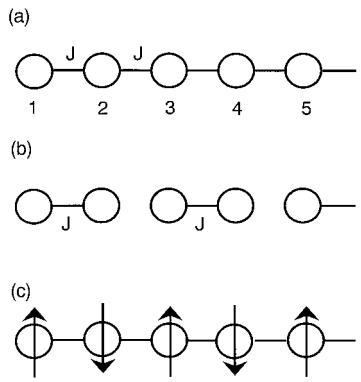

Figure 6. (a) A model describing a one-dimensional magnet interacting with nearest-neighbour exchange interaction (J). Circles show magnetic atoms. The numbers indicate the sites. (b) A model describing a dimerized singlet state. (c) A model describing the classical Néel state. Arrows show magnetic moments.

The low-energy excitation spectra of an $S = \frac{1}{2}$ 1D HAF have been calculated rigorously [15–17]. Figure 7 shows the theoretical excitation energy ($E(k)$) as a function of momentum k. No energy gap exists at the points $k = 0$ and π. The elementary excitation is a kink with

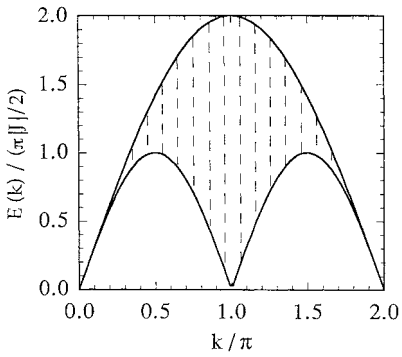

Figure 7. The theoretical excitation spectra of an $S = \frac{1}{2}$ one-dimensional Heisenberg antiferromagnet.

$S = \frac{1}{2}$ [17] now called a 'spinon'. The dispersion relation for the spinon excitation is given by [17]

$$E(k) = \frac{1}{2}\pi J \sin(k) \qquad 0 \leqslant k \leqslant \pi. \tag{10}$$

We can intuitively understand that the spinon excitation from the sea of the singlet ground state does not need to break the local exchange bonds (if we broke the bond locally, we would have an $S = 1$ excitation), so the excitation energy at $k = 0$ and π can be very small.

In 1983, Haldane [18] argued that the excitation spectrum of a 1D HAF with integer S ($=1, 2, 3, \ldots$) is radically different from that with half-odd-integer S ($=\frac{1}{2}, \frac{3}{2}, \frac{5}{2}, \ldots$). The former is expected to have an energy gap between the ground state and first excited one in contrast to the case for the latter. Haldane's argument is based on a field theoretical treatment of the 1D HAF problem and is not easy to understand for non-specialists. We will give an explanation for the existence of the energy gap (Haldane gap) later.

As was proposed by Affleck *et al* [19], the ground state of an integer-S 1D HAF is well described by the valence-bond-solid (VBS) model. This was confirmed experimentally by Hagiwara *et al* [20] as will be shown later. Figure 8(a) depicts the VBS state for $S = 1$. Spin 1 is obtained by symmetrization of two $S = \frac{1}{2}$ variables. The spin-singlet state can be written with two valence bonds emanating from each site and terminating at different sites. The existence of the energy gap can be understood intuitively as follows: when the strength of

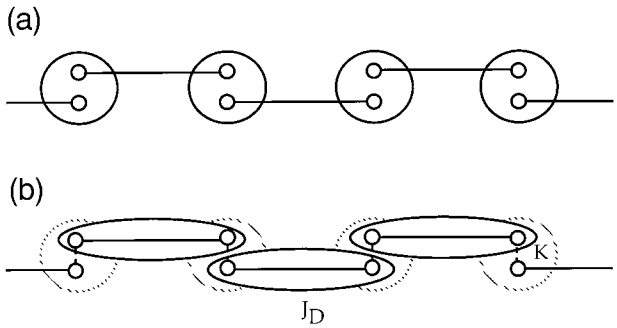

Figure 8. (a) Diagrammatic representation for the valence-bond-solid (VBS) ground state of an $S = 1$ one-dimensional Heisenberg antiferromagnet. The larger circles show the magnetic atoms with $S = 1$ and the smaller ones the $S = \frac{1}{2}$ variables. (b) The VBS state with $J_D \gg K$, where J_D is the valence bond and K is the force needed to align the two $S = \frac{1}{2}$ variables parallel to each other in a given atom.

the valence bond, J_D, is much larger than the force, K, needed to align the two $S = \frac{1}{2}$ variables in a given atom, the system can be viewed as a collection of antiferromagnetic dimers coupled by a weak ferromagnetic interaction as shown schematically in figure 8(b). In this case, the ground state is a singlet with a gap of $\sim J_D$ to the excited triplet as explained above. On increasing K relative to J_D, the gap energy will decrease and the triplet excitation will have a dispersion. There is no phase transition between the $S = \frac{1}{2}$ dimer and the $S = 1$ Haldane states [21]. Because of the quantum many-body effects, the Haldane gap energy (E_G) is given by $\sim 0.41J$ [22]. The most accurate value to date is obtained from an exact diagonalization as $E_G/J = 0.410\,49 \pm 2 \times 10^{-5}$ [23]. From a numerical calculation, Takahashi [24] showed that the energy gap at $k = 0$ is about two times larger than that at $k = \pi$. The value of the Haldane gap is shown to decrease with S as $E_G \sim JS^2 \exp(-\pi S)$ [18]. So, the observation of E_G becomes difficult at higher values of S.

Figure 9 shows schematically some typical examples of 1D and Q1D magnets. Figure 9(a) illustrates a 1D magnet interacting with the nearest-neighbour exchange J. A variant of figure 9(a) is shown in figure 9(b) in which the exchange interaction changes from J_1 to J_2 alternately. There are several variations for 1D magnets, e.g., a 1D magnet with alternating spin values S_1 and S_2, a 1D magnet with competing nearest-neighbour and next-nearest-neighbour exchange interactions and so on. In the latter case, a helical structure is expected for the classical spin. A quantum version of this model shows interesting properties [25–27].

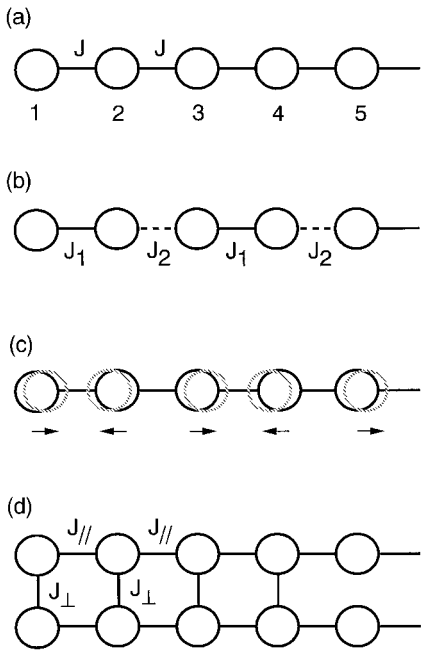

Figure 9. Schematic representations of some typical examples of one-dimensional and quasi-one-dimensional magnets.

In an insulating magnet, the exchange interaction depends greatly on the distance between the magnetic atoms. If an $S = \frac{1}{2}$ 1D HAF gains exchange energy by contracting the separation between magnetic atoms at the cost of lattice energy, the system shows a transition to a dimerized singlet ground state as shown schematically in figure 9(c). This is called a spin–Peierls transition. A number of organic materials exhibiting a spin–Peierls transition has

been reported [28]. In 1993, Hase *et al* [29] found the first inorganic material $CuGeO_3$ that exhibited a spin–Peierls transition. The advantage of this inorganic spin–Peierls material over the organic ones is that the former can be doped with many kinds of ion to form alloys such as $GeCu_{1-x}Zn_xO_3$, $GeCu_{1-x}Mg_xO_3$, $GeCu_{1-x}Ni_xO_3$ and $CuGe_{1-x}Si_xO_3$. A striking effect of the doping is that a small amount of impurity destroys the singlet ground state and induces an antiferromagnetic long-range ordering. The concentration, x, versus temperature phase diagram of $CuGe_{1-x}Si_xO_3$ obtained by Renard *et al* [30] is shown in figure 10.

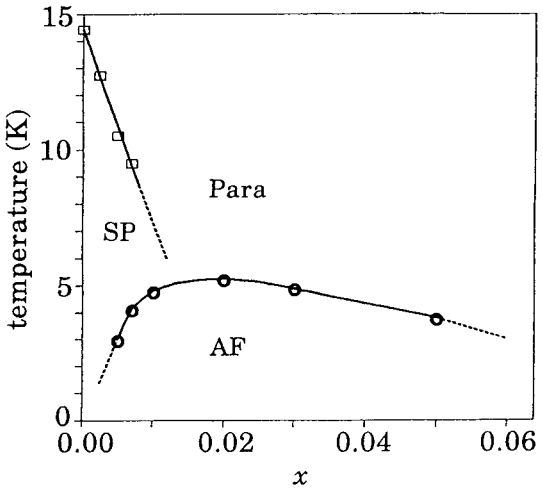

Figure 10. The concentration (x) versus temperature phase diagram of $CuGe_{1-x}Si_xO_3$. AF: antiferromagnetic phase; SP: spin–Peierls phase. (Figure from reference [30].)

The coexistence of lattice dimerization and antiferromagnetic ordering has been observed below the Néel temperature in $CuGe_{0.993}Si_{0.007}O_3$ [31] and in $Cu_{1-x}Zn_xGeO_3$ [32] by neutron scattering experiments. Fukuyama *et al* [33] presented a theory to explain the disorder-induced long-range antiferromagnetic ordering found in doped $CuGeO_3$. According to this theory, an edge spin is created at the Cu site which neighbours the impurities. This edge spin induces a staggered moment at the Cu sites whose amplitude decreases with the distance from the impurity. These magnetized chains interact with the neighbouring chains resulting in long-range ordering. The lattice dimerization can coexist with the magnetic ordering in such a way that the maximum displacement of the lattice occurs at the position where the staggered moment is at a minimum.

Figure 9(d) shows schematically a two-leg spin ladder, in which two 1D magnets are coupled with the exchange interaction $J_\perp$. The ground state of an $S = \frac{1}{2}$ antiferromagnetic two-leg ladder is a singlet with an energy gap to the lowest excited triplet [34]. Generally, $S = \frac{1}{2}$ antiferromagnetic spin ladders with even numbers of legs show the property mentioned above. On the other hand, the corresponding ladders with odd numbers of legs have no gap in the excitation spectrum [34]. The existence of an energy gap in the excitation spectrum of an $S = \frac{1}{2}$ two-leg antiferromagnetic ladder can be understood similarly to the case of the $S = 1$ 1D HAF. When $J_\perp \gg J_\parallel$ (>0), the system is viewed as a collection of almost independent $S = \frac{1}{2}$ dimers. In this case, the low-energy spectrum consists of a singlet ground state and an excited triplet with an energy gap of $\sim J_\perp$. Theoretical studies [35–39] showed that on decreasing $J_\perp$ relative to $J_\parallel$ the energy gap decreases and the triplet excitation has a dispersion due to the many-body quantum effect. The excitation energy has a minimum at $k = \pi$ whose

value is given by $0.504J_\perp$ for an isotropic ($J_\parallel = J_\perp$) two-leg ladder [40]. The energy gap at $k = \pi$ is commonly called a 'spin gap'.

On increasing the number of legs in the spin ladder, one approaches a 2D magnet. The energy gap deceases with the increase in the number of legs [34]. The ground state of an $S = \frac{1}{2}$ square-lattice HAF has been assumed [41] to be Néel ordered with a finite magnetic moment at each magnetic atom, aligned antiparallel to the moments on the neighbouring atoms. The elementary excitation from the Néel state is well approximated by spin waves. A small deviation in the magnetic moments from the fully aligned state propagates in the crystal like a wave, which is called a 'spin wave'. In the absence of anisotropy, the spin-wave spectrum has no gap at $k = 0$. Consequently, the relation between the frequency and magnetic field of the AFMR in a 2D HAF is the same as that for EPR.

The discovery of a high-temperature superconductor [42] has stimulated the study of 2D antiferromagnets. Yildirim *et al* [43] have made a detailed calculation of the electronic states of the lamellar copper oxides. They showed that there exists an in-plane as well as out-of-plane anisotropies even in a system with tetragonal symmetry originating from the combined effects of spin–orbit and Coulomb exchange interactions. As a result, one expects an in-plane spin-wave gap at $k = 0$ due to the quantum zero-point energy. Attempts to observe this in-plane gap using a neutron inelastic scattering technique [44] were not successful because the energy resolution near $k = 0$ in the sub-meV range (1 meV $\simeq$ 242 GHz) is not sufficient for this purpose if one uses thermal neutrons. A recent ESR measurement on the $S = \frac{1}{2}$ tetragonal Heisenberg antiferromagnets $Sr_2CuO_2Cl_2$ and $Sr_2Cu_3O_4Cl_2$ revealed clearly the existence of an energy gap of quantum origin [45].

4. ESR study on one-dimensional Heisenberg antiferromagnets

4.1. ESR in Haldane materials

We call Q1D Heisenberg antiferromagnets with integer S Haldane materials. The most extensively studied $S = 1$ Haldane material is $Ni(C_2H_8N_2)_2NO_2(ClO_4)$, abbreviated as NENP. Here, Ni^{2+} ($3d^8$) has spin 1. This compound crystallizes in the orthorhombic system [46]. The structure consists of $Ni(C_2H_8N_2)_2NO_2$ chains along the b-axis as shown in figure 11. These chains are well separated from each other by ClO_4 molecules.

The temperature dependence of the magnetic susceptibility of a single-crystal sample of NENP was measured by Renard *et al* [47]. The susceptibility shows a broad peak around 60 K, which is characteristic of lower-dimensional antiferromagnets, and a steep decrease at low temperatures. The latter behaviour is consistent with the presence of a singlet ground state and a gap to the lowest excited state in this compound. The magnetic parameters are determined to be [46] $|J|/k_B = 47.5$ K, $g_a = 2.23$, $g_b = 2.15$ and $g_c = 2.21$. From neutron inelastic scattering measurements, the inter-chain exchange interaction, J', is found to be much smaller than J ($|J'/J| = 4 \times 10^{-4}$) [47].

The first ESR experiment on a Haldane material was performed by Date and Kindo [48]. They observed an ESR signal at $\nu = 47.0$ GHz in a single-crystal sample of NENP. The temperature dependence of the intensity of this ESR signal is shown in figure 12. It is immediately clear that the ESR line comes from a transition within excited states, not from a ground state, for the reason given below. The intensity of ESR depends on the difference in thermal population between the energy levels pertaining to the ESR transition. If there is an energy gap between the ground and the lowest excited state, the thermal population of the excited state is larger at higher temperature. On the other hand, the difference in thermal population within the excited states becomes small with increasing temperature. Consequently,

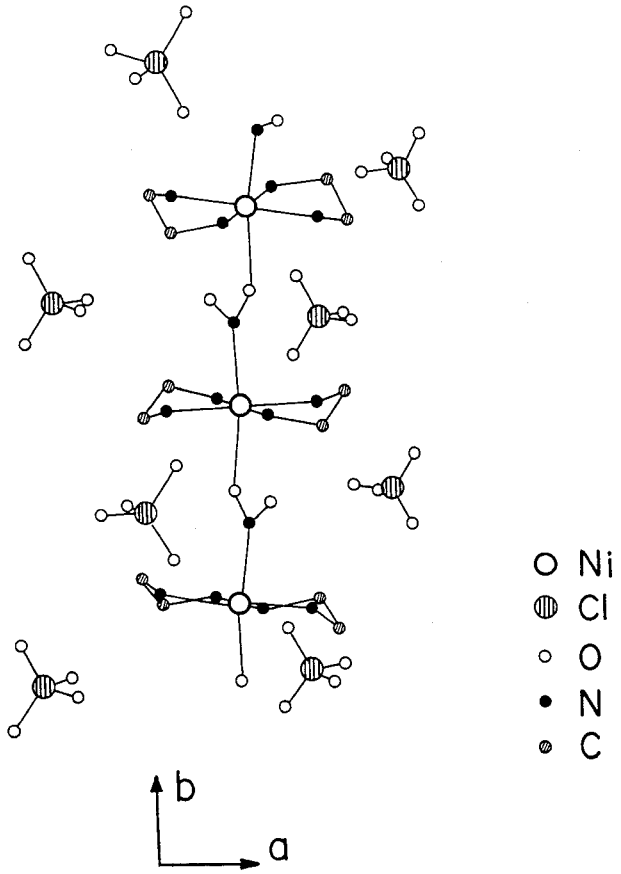

Figure 11. The crystal structure of $Ni(C_2H_8N_2)_2NO_2(ClO_4)$, abbreviated as NENP.

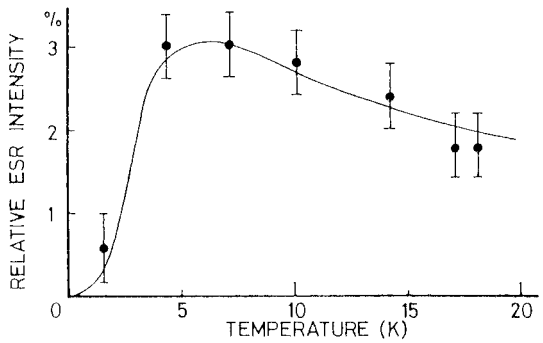

Figure 12. The temperature dependence of the ESR intensity in NENP. (Figure from reference [48].)

the intensity of the ESR transition within the excited states exhibits a peak at a finite temperature as is seen from figure 12. The result of the ESR measurement was analysed on the basis of the energy level scheme proposed to explain the behaviour of the magnetization of NENP in high magnetic fields [49].

As described in section 3, the first excited state of an $S = 1$ 1D HAF is a triplet. Due to the crystal structure, single-ion anisotropy terms such as DS_z^2 and $E(S_x^2 - S_y^2)$ are present for NENP. In the following discussion, we neglect the E-term because it is much smaller than the D-term.

In figure 13 we show the energy level scheme for an $S = 1$ 1D HAF. Figure 13(a) depicts the singlet ground state and first excited triplet of the unperturbed system. When D (>0) is introduced, the triplet state splits into a lower doublet and a higher singlet [50] as shown in figure 13(b). Note that the splitting of the triplet state by the D-term in the $S = 1$ 1D HAF is opposite to the case for an isolated $S = 1$ ion in a tetragonal crystal field. We start from the energy level scheme in figure 13(b) and apply the conventional one-ion crystal-field theory to discuss the field dependence, although the energy levels originate from quantum many-body effects. On applying $\boldsymbol{B}$ parallel to the z-axis (the quantization axis of the D-term), the triplet state Zeeman splits as in figure 13(c). When $\boldsymbol{B}$ is applied perpendicularly to $\boldsymbol{z}$ ($\boldsymbol{B} \parallel \boldsymbol{x}$), the energy levels depend non-linearly on B as shown in figure 13(d). The energy levels in figures 13(b) and 13(c) are specified by the z-component of the total spin, S_z^{tot}. For the singlet ground state $S_z^{\mathrm{tot}} = 0$, and for the triplet state $S_z^{\mathrm{tot}} = \pm 1$ and 0. ESR transitions are possible within the triplet states whose S_z^{tot}-values differ by ± 1 as in ordinary ESR. In the case of figure 13(d), all of the transitions within the excited states become possible because of the mixing.

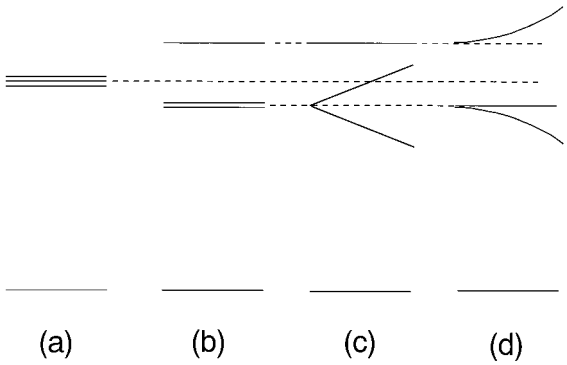

Figure 13. The energy level scheme for an $S = 1$ one-dimensional Heisenberg antiferromagnet. (a) The singlet ground state and first excited triplet in an isotropic case and in zero field. (b) Those with the single-ion D-term in zero field. (c), (d) Effects of the external magnetic field on (b).

Field theoretic treatments of the excited triplet in an applied magnetic field have been reported [51,52]. Golinelli *et al* [53] made exact-diagonalization and perturbation calculations on the lowest excited triplet of an $S = 1$ 1D HAF. These theoretical studies gave essentially the same result as that shown in figure 13.

The field dependence of the lowest triplet in NENP has been measured directly by neutron inelastic scattering experiments. Figure 14 shows the result obtained by Regnault *et al* [54] at $k = \pi$ and $T = 1.4$ K for $\boldsymbol{B}$ parallel to the c-axis. Qualitatively, the behaviour of the energy levels in the field $\boldsymbol{B}$ is the same as in figure 13(d). The small splitting between the modes denoted by X and Y at $B = 0$ in figure 14 comes from the single-ion anisotropy E-term.

Surprisingly, the ESR transitions from the singlet ground state to the excited triplet which are forbidden by the momentum conservation law (for the ground state $k = 0$ and for the lowest excited triplet $k = \pi$) have also been observed in NENP [55–58] and a related compound $Ni(C_3H_{10}N_2)_2NO_2(ClO_4)$ (NINO) [57, 58]. Figure 15 shows the most complete

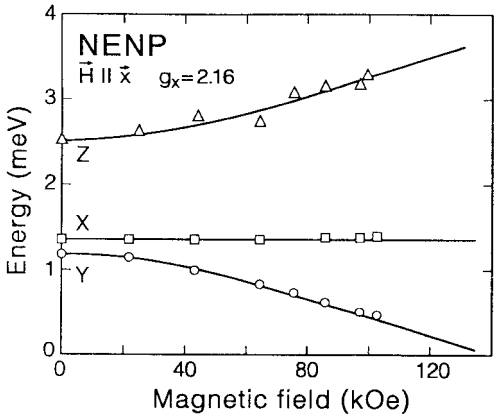

Figure 14. The magnetic field dependence of the first excited triplet in NENP obtained from the neutron inelastic scattering measurements. The external field is applied perpendicularly to the chain axis. (Figure from reference [54].)

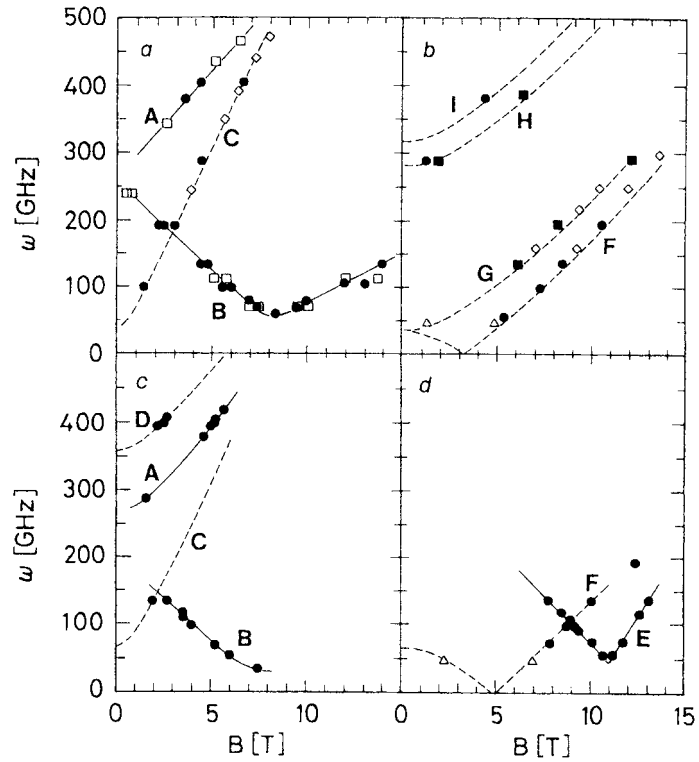

Figure 15. Frequency versus magnetic field plots of the ESR positions observed in (a) NENP, $\boldsymbol{B} \parallel \boldsymbol{b}$, (b) NENP, $\boldsymbol{B} \parallel \boldsymbol{a}, \boldsymbol{c}$, (c) NINO, $\boldsymbol{B} \parallel \boldsymbol{b}$, (d) NINO, $\boldsymbol{B} \parallel \boldsymbol{c}$. (Figure from reference [57].)

frequency–field plots to date for the ESR points for NENP and NINO [57]. The ESR transitions from the ground state can be identified from the temperature dependence of the intensity, because the ESR intensity from the ground state increases with decreasing temperature.

Two theories [59, 60] were presented to explain these unexpected ESR transitions. If one looks at figure 11 carefully, one recognizes that there are two crystallographically inequivalent sites for Ni^{2+} ions with one of the principal axes of the octahedron tilted away from the b-axis to either side when one moves from one site to another along the b-axis. When the external magnetic field is applied along the b-axis, this tilting of the crystal-field axis causes a staggered field at each Ni^{2+} site [61]. This staggered magnetic field mixes the state at $k = 0$ with that at $k = \pi$, thereby making the transitions from the ground state to the excited triplet possible. A polarization analysis of the ESR absorption in NINO [62] has confirmed the theoretical prediction. A small difference in the Haldane gap energy has been reported between that determined from the neutron inelastic scattering and that from ESR experiments [57].

Usually, Q1D magnets exhibit a long-range ordering (LRO) at a finite temperature [13] due to the inter-chain interaction. The compound NENP does not show any indication of LRO down to 300 μK [63], whereas the Q1D HAF $CsNiCl_3$ shows LRO at $\sim$4.7 K [64]. The difference in behaviour between the two compounds comes from the difference in the strength of J'. How robust is the Haldane phase in a Q1D HAF against perturbation? Sakai and Takahashi [65] studied theoretically an $S = 1$ Q1D HAF with a single-ion anisotropy. Figure 16 shows the phase diagram in the D–J' plane at $T = 0$ K [65], where z is the number of neighbouring chains. We see that the Haldane phase (denoted by 'H disorder' in figure 16) exists for a rather wide range of anisotropy and J'-values.

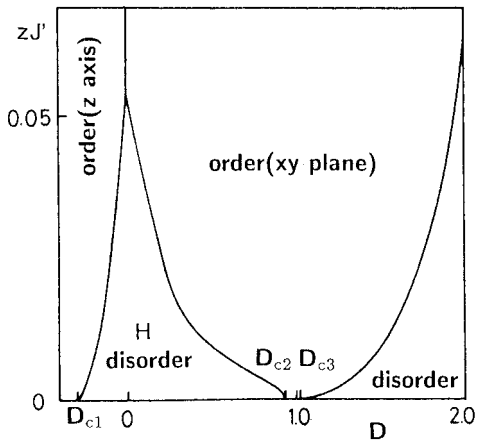

Figure 16. The theoretical phase diagram for an $S = 1$ quasi-one-dimensional Heisenberg antiferromagnet with single-ion anisotropy. (Figure from reference [65] with a small change in the labelling for consistency with the text.)

As reported before [49], strong magnetic fields destroy the Haldane gap and the system recovers magnetism. Then, we expect LRO to occur in a Q1D $S = 1$ HAF under high fields and at low temperatures. This was demonstrated experimentally by Honda *et al* [66] for $Ni(C_5H_{14}N_2)_2N_3(PF_6)$ (NDMAP). The value of J for NDMAP is determined to be 30.0 K [66], which is considerably smaller than that of NENP. So, a heat capacity measurement—which is one of the best methods for confirming the occurrence of LRO—can be done with a commercial superconducting magnet.

Figure 17 shows the $B(H)$–T phase diagram of NDMAP determined from the heat capacity measurement [66]. The low-T and high-B region above the boundary corresponds to the LRO phase in the respective field direction. The anisotropy in the phase boundary is explained as

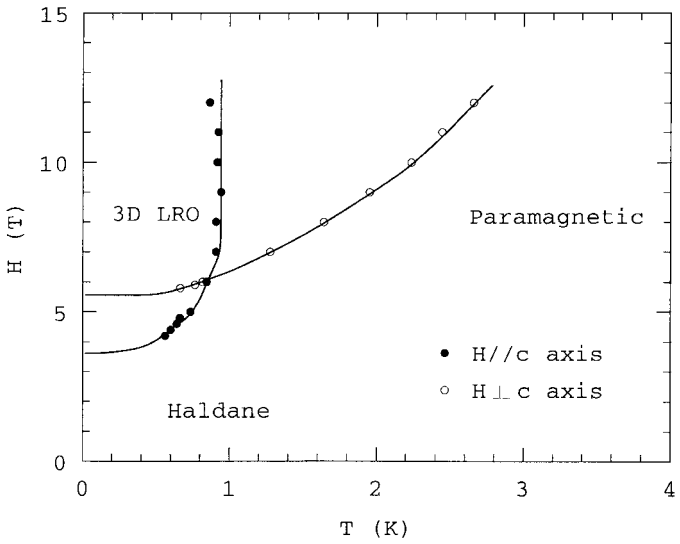

Figure 17. The magnetic field versus temperature phase diagram of the $S = 1$ quasi-one-dimensional antiferromagnet $Ni(C_5H_{14}N_2)_2N_3(PF_6)$. (Figure from reference [66].)

follows. Because the sign of the single-ion anisotropy constant D is positive, spins in the ordered phase lie in a plane perpendicular to the c-axis of the crystal, which is the quantization axis of D. When $\boldsymbol{B}$ is applied parallel to the c-axis, the XY symmetry is retained. On the other hand, when $\boldsymbol{B}$ is applied perpendicularly to the c-axis, the XY symmetry is broken and an Ising anisotropy is produced. It is widely accepted that the phase transition temperature of an Ising system is higher than that of an XY system for a given space dimensionality.

Figure 18 shows the results of ESR measurements made on a single crystal of NDMAP at $T = 1.7$ K for $\boldsymbol{B} \parallel b$-axis [67]. These experimental points constitute two excitation branches. Here, H_{LRO} is the field at the transition from the disordered to the LRO phase at $T = 1.7$ K (figure 17). Since we expect an antiferromagnetic arrangement of spins to exist in the LRO phase, one of these two branches must be identified as an AFMR mode. Due to the single-ion anisotropy D-term ($D > 0$), spins in the LRO phase are confined to a plane perpendicular to the c-axis. A small anisotropy coming from the single-ion E-term determines the easy axis in this plane, provided that we neglect the effects of dipole–dipole interaction. The branch labelled 'AFMR' was assigned to the AFMR mode from the temperature dependence of the resonance point which showed a sudden change around T_{N}. The frequency versus magnetic field relation of the AFMR branch was found to be well fitted with the following formula proposed by Magariño *et al* [68] for analysing the AFMR mode in the quasi-1D $S = 5/2$ HAF $(CH_3)_4NMnCl_3$ (TMMC):

$$2\pi\nu/\gamma = g_{\perp}\mu_{\mathrm{B}}\{(B - B_0)^2 - C\}^{1/2} \tag{11}$$

where B_0 is a constant which was introduced to include a quantum effect on the AFMR frequency [68] and C is a constant. From a fitting of equation (11) to the experimental data (figure 18), $B_0 = 2.0$ T and $C = 14.5$ T^2 have been obtained. Osano *et al* [69] have calculated the magnon spectra of TMMC in a magnetic field taking into account the non-linear couplings among magnons (quanta associated with spin waves). The value of B_0 obtained for NDMAP is larger than that for TMMC. This shows that the quantum fluctuation in a quasi-1D HAF becomes more prominent with decreasing S-value. The constant C in equation (11) is given

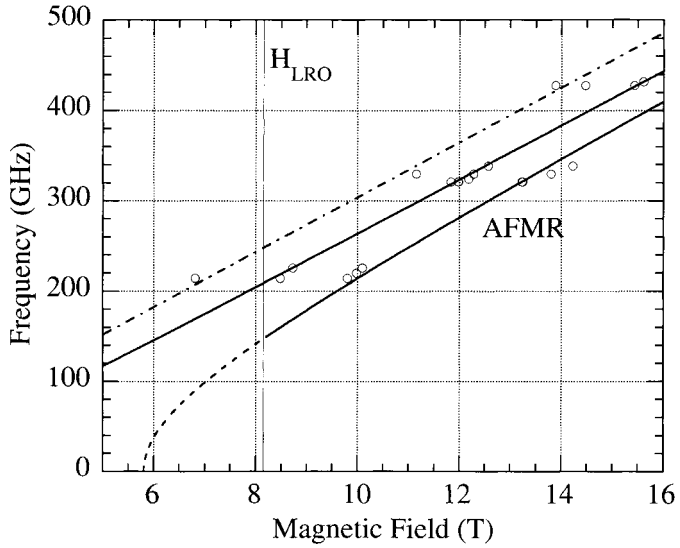

Figure 18. The ESR signals observed in the long-range-ordered phase of $Ni(C_5H_{14}N_2)_2N_3(PF_6)$ are plotted in the frequency–magnetic field plane. The dot–dashed line represents the EPR one with $g = 2.17$ along which a weak signal has been observed. (Figure from reference [67].)

by $C = 2B_E B_A$ [10]. Using the value $J/k_B = 30.0$ K determined before [66], $B_A = 0.18$ T ($g\mu_B B_A/k_B = 0.26$ K) is obtained. The ESR transitions from the ground state have not been observed in NDMAP. This is consistent with the fact that only one site exists for Ni^{2+} in this compound, so no staggered field is induced under applied magnetic fields.

4.2. Observing an $S = \frac{1}{2}$ degree of freedom in an $S = 1$ 1D HAF by means of ESR

As is explained in section 3, the VBS model [19] has been proposed to describe the ground state of an $S = 1$ 1D HAF. The idea for testing the validity of the VBS model experimentally was as follows [20]: as is shown in figure 19(b), when a host atom is substituted for with an impurity atom, the valence bonds will be broken at the impurity sites if the exchange

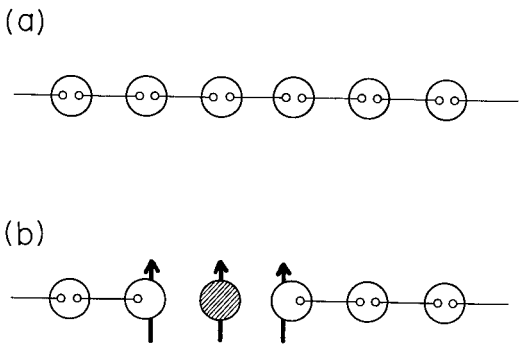

Figure 19. (a) As figure 8(a). (b) A host atom is substituted for with an impurity, resulting in spin-$\frac{1}{2}$ states at host sites neighbouring the impurity. The arrows show the spin moment. (Figure from reference [20].)

interaction between the host and impurity spins is sufficiently weak. This will result in an $S = \frac{1}{2}$ degree of freedom at the host spin sites neighbouring the impurity. ESR measurements were performed on a single crystal of NENP containing $\simeq$0.7 at.% Cu^{2+} impurity [20]. Three ESR lines are observed at the X and K ($\sim$22 GHz) bands at 4.2 K, whose intensities decrease rapidly with increasing temperature. From these observations, it is evident that the ESR lines do not come from free Cu^{2+} ions isolated from the chains. Then, it is natural to invoke a weak exchange coupling between Ni^{2+} and Cu^{2+} spins. The following two cases should be considered: (i) $Ni^{2+}(S = 1)$–Cu^{2+}–$Ni^{2+}(S = 1)$ and (ii) $Ni^{2+}(S = \frac{1}{2})$–Cu^{2+}–$Ni^{2+}(S = 1/2)$. Here, Cu^{2+} is assumed to have $S = \frac{1}{2}$ as is generally accepted. Since the value of D for Ni^{2+} in NENP is $\simeq$12 K [70], the ESR frequency and field expected for case (i) are much higher than those observed in this experiment. So, only case (ii) is possible. The results of the ESR measurements were analysed with the following Hamiltonian when $\boldsymbol{B}$ is applied along the b-axis:

$$H = -2[J_c(S_1^x + S_2^x)s^x + J_a(S_1^y + S_2^y)s^y + J_b(S_1^z + S_2^z)s^z] + G_b\mu_B B(S_1^z + S_2^z) + g_b\mu_B B s^z \tag{12}$$

where, J_a, J_b and J_c are, respectively, the components along the crystallographic a-, b- and c-axes of the exchange interaction between the host and impurity spins, S_1 and S_2 the $\frac{1}{2}$-spin degrees of freedom induced at the host sites, s the impurity spin, G_b the g-value along the b-axis of the $S = \frac{1}{2}$ degrees of freedom and g_b the g-value of the impurity spin parallel to the b-axis. Note that no D-term is possible for $S = \frac{1}{2}$. The Hamiltonian when $\boldsymbol{B}$ is applied parallel to the a- or c-axes is given similarly. The eigenvalues of equation (12) are plotted against B in figure 20. Here, the following values of the parameters have been used: $J_a = 0.79$ cm^{-1}, $J_b = 0.67$ cm^{-1}, $J_c = 0.83$ cm^{-1}, $G_b = 2.15$ and $g_b = 2.24$. The broken lines in figure 20 show the allowed transitions for the microwave frequencies at 9.25 GHz and 21.7 GHz obtained from a calculation of the probabilities of transition between the energy

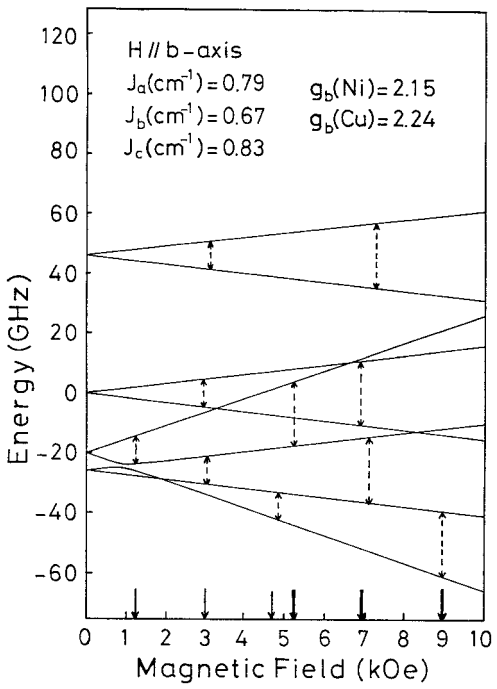

Figure 20. The eigenvalues of equation (12) are plotted versus the external magnetic field applied along the b-axis.

levels. The experimental results observed at the same frequencies are also shown by the thin and thick arrows. We see that the agreement between theory and experiment is satisfactory. The angular dependence of the ESR positions is also satisfactorily explained. The Hamiltonian (equation (12)) is phenomenological. Kaburagi and Tonegawa [71] have calculated low-lying excited states of an $S = 1$ 1D HAF with an $S = \frac{1}{2}$ impurity by means of variational methods and numerical diagonalization. They showed that equation (12) can be derived from the ordinary Hamiltonian and that the origin of the anisotropy in the exchange interactions ($J_b \neq J_a \simeq J_c$) can be explained as arising from the D-term. Given the energy levels, one can calculate the magnetic properties, e.g., the magnetization curve, of this system at low temperatures. It has been shown that the magnetization curve observed for NENP:Cu^{2+} is quantitatively reproduced by a calculation without any adjustable parameters [72].

The fractional $S = \frac{1}{2}$ states have also been observed in NENP doped with non-magnetic atoms such as Zn, Cd and Hg [73] and in Y_2BaNiO_5 [74]. In the latter sample, a few per cent of Ni^{2+} are substituted for with Ni^{3+} with $S = \frac{1}{2}$ due to an excess of oxygen.

As is described above, the ground state and low-lying excited states of an $S = 1$ 1D HAF with an impurity are well described by the presence of the $S = \frac{1}{2}$ degrees of freedom at the chain ends, thus giving strong evidence for the VBS model as a good description of the ground state. Miyashita and Yamamoto [75] have made a quantum Monte Carlo study of the finite $S = 1$ 1D HAF and shown that a staggered moment appears in the chain, the magnitude of which decays exponentially with the distance from the chain ends.

4.3. ESR in pure and doped $CuGeO_3$

As described in section 3, $CuGeO_3$ is the first inorganic material found to exhibit a spin–Peierls transition. This compound crystallizes in the orthorhombic system with the Cu–O–Cu chains along the c-axis [29].

The $B(H)$–T phase diagram of $CuGeO_3$ determined from magnetization measurements is shown in figure 21 [76]. We have the three phases denoted by D, U and M. The boundary line separating the M and U phases has been supplemented by ac susceptibility measurements [77]. Hase *et al* [76] claimed that the $B(H)$–T phase diagram of $CuGeO_3$ is qualitatively the same as those obtained for organic spin–Peierls compounds [28]. In the D phase, the system is in the dimerized state shown schematically in figure 9(c) with spin-singlet and lattice dimerization. In the U phase, the system is in an $S = \frac{1}{2}$ Q1D HAF state without lattice distortion. The M phase is in a magnetized state with an incommensurate lattice distortion whose wave vector changes with B [78, 79]. The magnetized chains consist of singlet dimers separated by a domain wall forming a soliton lattice [79]. The existence of the magnetic soliton lattice was confirmed from Cu NMR in $CuGeO_3$ up to $\sim$17 T [80]. A synchrotron x-ray scattering experiment in high magnetic fields showed that the lattice modulation has the form of a soliton lattice [81].

Brill *et al* [82] have made ESR measurements on $CuGeO_3$ in the D phase. They observed two kinds of ESR signal, whose intensities behaved differently with varying temperature. The intensity of one increases with decreasing temperature, while that of the other shows a broad peak at a finite temperature. This behaviour of the ESR signals in $CuGeO_3$ is very similar to the one observed for NENP (see section 4.1).

An antiferromagnetically coupled $S = \frac{1}{2}$ dimer exhibits the energy level scheme shown on the right-hand side of figure 5. On applying an external magnetic field, the excited triplet Zeeman split and ESR transitions within the triplet whose intensities show a broad peak in the temperature dependence are possible. Although the D phase in a spin–Peierls system originates from many-body quantum effects, one expects the D phase to have essentially the same energy level scheme as an isolated dimer.

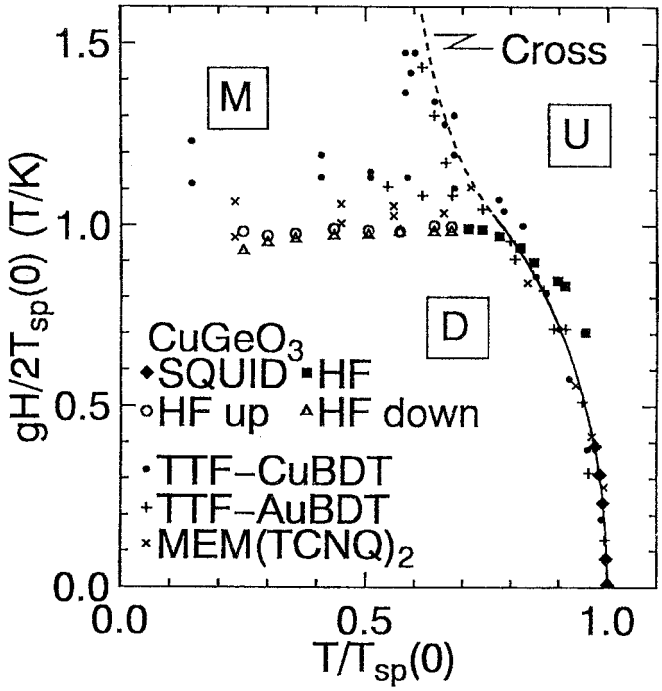

Figure 21. The temperature versus magnetic field phase diagram of $CuGeO_3$. D: dimerized phase; M: mixed phase; U: uniform phase. (Figure from reference [76].)

The observation of an ESR signal whose intensity increases with decreasing temperature means that this signal is caused by a transition from the ground state to the excited triplet. This transition is forbidden for an ordinary Hamiltonian. A mechanism which makes this transition possible has been proposed [83] which invokes the Dzyaloshinsky–Moriya interaction.

The ESR technique has been used to elucidate the disorder-induced long-range ordering in this spin–Peierls system. Figure 22 shows the results of ESR measurements made on a single-crystal sample of $Cu_{0.96}Zn_{0.04}GeO_3$ [84]. Here, the angular frequency, ω, is divided by the magneto-mechanical ratio, γ, to express it in magnetic field units ($\omega/\gamma = 1$ T corresponds to 28.0 GHz with $g = 2.00$) and the external magnetic field, B, is scaled by the g-value parallel to the a-, b- or c-axes for the respective field directions. It is clear that we have observed ESR signals from a magnetically ordered phase, not from the D phase, because the frequency–field relation of the ESR in the D phase [82, 83] is completely different from that shown in figure 22. Comparing the frequency–field chart in figure 22 with that of the uniaxial antiferromagnet MnF_2 shown in figure 2, we see a similarity between the two, except that there are two ESR frequencies at $B = 0$ and the resonant frequency depends non-linearly on B for $Cu_{0.96}Zn_{0.04}GeO_3$. The experimental results given in figure 22 are explained by the theory of AFMR [10] with orthorhombic anisotropy. From a comparison between theory and experiment, one finds that the easy, second easy and hard axes are parallel to the c-, a- and b-axes, respectively. The full, dotted and dash–dotted lines in figure 22 are theoretical ones [10] with $K_1/\chi_\perp \simeq 0.45$ T^2 and $K_2/\chi_\perp \simeq 1.05$ T^2, where K_1 and K_2 are the anisotropy constants.

Antiferromagnetic resonance has been observed also in $CuGe_{1-y}Si_yO_3$ [85] and in $Cu_{1-x}Ni_xGeO_3$ [86].

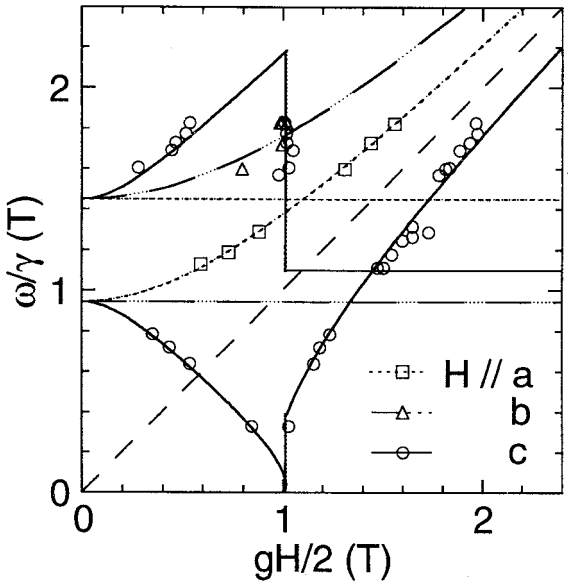

Figure 22. The frequency versus magnetic field plots of the resonance points at 1.7 K in a single-crystal sample of $Cu_{0.96}Zn_{0.04}GeO_3$. Open squares, triangles and circles denote experimental data and dotted, dash–dotted and full curves are theoretical ones for $\boldsymbol{B} \parallel a$-, b- and c-axes, respectively. (Figure from reference [84].)

5. ESR in more complex systems

The $S = 1$ 1D HAF with bond alternation shown schematically in figure 9(b) exhibits interesting properties. As discussed theoretically by Singh and Gelfand [87], this system shows a transition from the Haldane phase to a dimerized one at the critical value of J_1/J_2 (or J_2/J_1) $\sim$0.6. Tonegawa *et al* [88] studied numerically the same system with single-ion anisotropy and magnetic fields, where the critical value is given as $\simeq$0.6 for $D = B = 0$. We can understand these theoretical results qualitatively as follows. When $J_1 = J_2$ the system is in the Haldane state. On the other hand, when either $J_1 \gg J_2$ or $J_2 \gg J_1$, the system can be viewed as a collection of almost independent antiferromagnetic dimers. So, there is a transition from the Haldane to the dimerized phase at a critical value of J_1/J_2.

Several $S = 1$ Q1D antiferromagnets with bond alternation have been synthesized [89, 90]. Narumi *et al* measured the magnetization of an $S = 1$ Q1D antiferromagnet with bond alternation, $Ni_2(Medpt)_2(\mu\text{-ox})(\mu\text{-}N_3)ClO_4{\cdot}0.5H_2O$, [91], where Medpt represents methylbis(3-aminopropyl)amine. The result is shown in figure 23. The magnetization is very small below $\sim$15 T and begins to increase at $\sim$17 T as was observed in $S = 1$ Haldane materials [49]. A new finding is that M is almost independent of B between 43 and 55 T, above which M begins to increase again. The value of M in the intermediate phase is half of the saturation magnetization.

The appearance of the plateau in the magnetization curve of an $S = 1$ 1D antiferromagnet with bond alternation is explained qualitatively as follows. We consider two limiting cases. First, let us start with the VBS model shown in figure 8(a). In the present case, because of the bond alternation, the critical field, B_T, at which the Haldane gap is destroyed is related mainly to the weaker exchange interaction (say, J_1). Above $B > B_T$ the singlet bonds connected by J_1 are gradually broken with increasing field and finally an $S = \frac{1}{2}$ degree of freedom appears

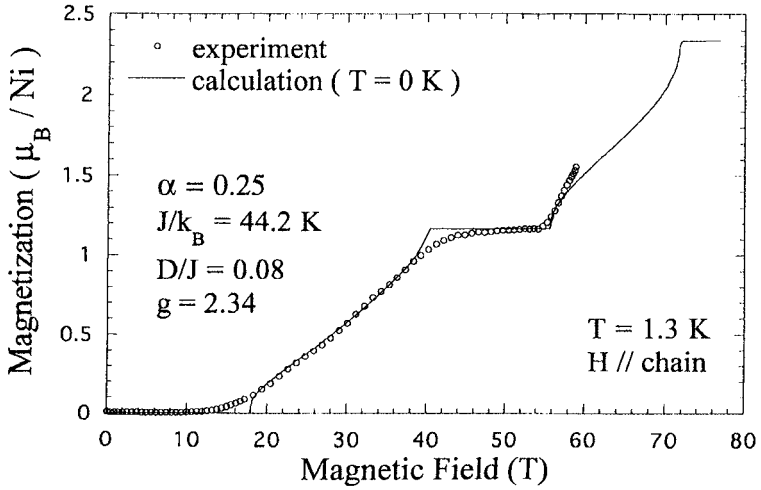

Figure 23. The magnetization curve of the $S = 1$ quasi-one-dimensional antiferromagnet with bond alternation $Ni_2(Medpt)_2(\mu\text{-ox})(\mu\text{-}N_3)ClO_4{\cdot}0.5H_2O$. (Figure from reference [91].)

at each atomic site. Then, the magnetization stays constant until the second gap, determined mainly by J_2, closes. This gives the plateau in the magnetization curve whose value is half of the saturation magnetization. On increasing B further, the singlet bonds connected by J_2 are gradually broken as B increases up to saturation.

If we start with isolated $S = 1$ antiferromagnetic dimers coupled by J_2, we have a singlet ground state, first excited triplet with $S^{\text{tot}} = 1$ and the highest quintuplet with $S^{\text{tot}} = 2$. The triplet lies above the ground state by J_2 and the quintuplet by $3J_2$. When B is applied to this system, the triplet and quintuplet states Zeeman split. The energy level of the excited triplet with $S_z^{\text{tot}} = -1$ decreases with B and finally crosses the ground state where the magnetization increases from zero to half of the saturation magnetization. This state stays unchanged until the energy level of the excited quintuplet with $S_z^{\text{tot}} = -2$ crosses the ground state at which the magnetization saturates. In this case, we expect a stepwise transition to occur at the two critical fields. Figure 23 shows that in a real system the transition is rather gradual, which reflects quantum many-body effects due to J_1.

An ESR study on $S = 1$ bond-alternating chains should give important information on the ground state. Narumi *et al* [92] claimed that the ground state is the $S = 1$ dimer state from their ESR measurements on the $S = 1$ antiferromagnetic bond-alternating chain compound $[Ni(333\text{-tet})(\mu\text{-}NO_2)](ClO_4)$ doped with a small amount of Zn.

Several copper oxides which can be regarded as a spin-ladder materials were synthesized [93]. Azuma *et al* [94] showed from magnetic susceptibility measurements that the $S = \frac{1}{2}$ two-leg-ladder material $SrCu_2O_3$ has a spin gap of $\sim$420 K. In principle, one can observe the ESR transitions within the excited triplet at high temperatures corresponding to the spin gap. The compound $Sr_{14}Cu_{24}O_{41}$ has two types of building block. One is simple chains of Cu ions and the other is two-leg ladders of Cu ions. A novel dimerized state has been found in the chain part of $Sr_{14}Cu_{24}O_{41}$ by ESR [95] and neutron inelastic scattering [96] experiments. This dimerized state originates from an interplay between spin and charge. The compound NH_4CuCl_3 has a ladder-like structure and exhibits two plateaus in the magnetization curve at $B_{c1} < B < B_{c2}$ and $B_{c3} < B < B_{c4}$ [97]. Several ESR lines have been observed in the respective phases in magnetic fields [98].

Recently, new Q2D materials with singlet ground states and energy gaps to the excitation such as CaV_4O_9 [99] and $SrCu_2(BO_3)_2$ [100] have been discovered. ESR transitions from the singlet ground state to the excited triplets have been observed in the latter material [101].

In the 1980s there was great progress in the understanding of random magnetism. In particular, spin glasses [102] and random magnets with competing spin anisotropies [103, 104] were intensively studied. The ESR method has been used to elucidate the magnetic properties of the latter system [105].

There is a large amount of ESR information on ABX_3-type triangular lattice antiferromagnets, where A stands for alkaline metal, B for the 3d transition metal and X for halogen atoms. Generally these materials show successive magnetic transitions due to frustration. In the ordered phases, the magnetic structure is more complex than that of conventional antiferromagnets. Therefore, one needs three or six sublattices to describe the magnetic properties of these systems. Several ESR signals corresponding to the motions of these multisublattices have been observed [106].

Molecular magnetic cluster complexes like $[Fe_8O_2(OH)_{12}(C_6H_{15}N_3)_6]Br_7(H_2O)Br{\cdot}H_2O$ and $[Mn_{12}O_{12}(CH_3COO)_{16}(H_2O)_4]{\cdot}2CH_3COOH{\cdot}4H_2O$ have attracted much attention in recent years, because these samples show a macroscopic quantum tunnelling phenomenon [107]. In these materials, the ground state has a total spin $S_{tot} = 10$ and they exhibit a complicated energy level scheme due to the presence of the single-ion anisotropy term. ESR is best suited for determining the energy levels because the energy resolution is much better than that of neutron scattering determinations. ESR measurements made on these materials [108–111] have revealed the energy level scheme.

6. Summary

We have reviewed the recent progress in the study of magnetic materials using a high-frequency ESR technique. First, we saw how useful high-frequency ESR is for studying antiferromagnetic materials, where the ESR frequency and magnetic field depend greatly on the exchange interaction and anisotropy energy of the materials. Next, we reviewed recent high-frequency ESR experiments made on $S = 1$ Haldane materials and the spin–Peierls system $CuGeO_3$. Then, we reviewed ESR studies performed on more complex systems, such as an $S = 1$ Q1D antiferromagnet with bond alternation, spin-ladder compounds and Q2D magnets. Each of these systems has a singlet ground state of quantum origin and an energy gap to the lowest excited state. On applying an external magnetic field, the system shows a transition from the non-magnetic to a magnetized state, and in some cases, long-range magnetic ordering occurs. I have tried to explain the nature of the singlet ground states and the behaviour in applied magnetic fields intuitively at the expense of rigour. I hope that this will be helpful to a broad audience in providing an understanding of the underlying physics.

Acknowledgments

I would like to thank M Hagiwara, A Harrison, B Lüthi and H-J Mikeska for reading the manuscript and for giving many useful comments. I have benefited from conversations with I Affleck, J P Boucher, M Date, B I Halperin, I Harada, M Hase, Z Honda, the late O Kahn, M Matsuda, S Miyashita, J P Renard, J Tuchendler and I Yamada.

This work was partially supported by the MR Science Research Programme of RIKEN and a Grant-in-Aid for Scientific Research from the Japanese Ministry of Education, Science, Sports and Culture.

References

[1] Zavoisky E 1945 *Fiz. Zh.* **9** 211
Zavoisky E 1945 *Fiz. Zh.* **9** 245
[2] Purcell E M, Torrey H C and Pound R V 1946 *Phys. Rev.* **69** 37
[3] Bloch F, Hansen W W and Packard M 1946 *Phys. Rev.* **70** 474
[4] For a review of EPR study in chemistry see
Gatteschi B D 1990 *Electron Paramagnetic Resonance of Exchange Coupled Systems* (Berlin: Springer)
Turek P 1999 *Magnetic Properties of Organic Materials* ed P M Lahti (New York: Dekker) ch 24, p 491
[5] Lynch W, Earle K and Freed J 1988 *Rev. Sci. Instrum.* **59** 1345
Muller F, Hopkins M A, Coron N, Grynberg M, Brunel L C and Martinez G 1989 *Rev. Sci. Instrum.* **60** 3681
[6] For a review of early work on antiferromagnetic resonance, see
Foner S 1963 *Magnetism* vol 1, ed G T Rado and H Suhl (New York: Academic) p 383
[7] The magnetic data for transition metal halides are found in
Katsumata K 1994 *Landolt–Börnstein New Series* Group III, vol 27j1, ed H P J Wijn (Berlin: Springer) p 1
[8] Hagiwara M, Katsumata K, Yamada I and Suzuki H 1996 *J. Phys.: Condens. Matter* **8** 7349
[9] Hagiwara M, Katsumata K, Yamaguchi H, Tokunaga M, Yamada I, Gross M and Goy P 1999 *Int. J. Infrared Millimeter Waves* **20** 617
[10] Nagamiya T, Yosida K and Kubo R 1955 *Adv. Phys.* **4** 1
[11] Ogasahara A and Miyashita S 2000 *Preprint*
[12] Bethe H 1931 *Z. Phys.* **71** 205
[13] For a review see
de Jongh L J and Miedema A R 1974 *Experiments on Simple Magnetic Model Systems* (London: Taylor and Francis)
[14] Anderson P W 1973 *Mater. Res. Bull.* **8** 153
[15] des Cloizeaux J and Pearson J J 1962 *Phys. Rev.* **128** 2131
[16] Müller G, Thomas H, Beck H and Bonner J C 1981 *Phys. Rev.* B **24** 1429
[17] Faddeev L D and Takhtajan L A 1981 *Phys. Lett.* A **85** 375
[18] Haldane F D M 1983 *Phys. Lett.* A**93** 464
Haldane F D M 1983 *Phys. Rev. Lett.* **50** 1153
[19] Affleck I, Kennedy T, Lieb E H and Tasaki H 1987 *Phys. Rev. Lett.* **59** 799
Affleck I, Kennedy T, Lieb E H and Tasaki H 1988 *Commun. Math. Phys.* **115** 477
[20] Hagiwara M, Katsumata K, Affleck I, Halperin B I and Renard J P 1990 *Phys. Rev. Lett.* **65** 3181
[21] Kolezhuk A K and Mikeska H-J 1997 *Phys. Rev.* B **56** R11 380
[22] Nightingale M P and Blöte H W J 1986 *Phys. Rev.* B **33** 659
[23] Golinelli O, Jolicoeur Th and Lacaze R 1994 *Phys. Rev.* B **50** 3037
[24] Takahashi M 1989 *Phys. Rev. Lett.* **62** 2313
[25] Majumdar C K and Ghosh D K 1969 *J. Math. Phys.* **10** 1399
[26] Haldane F D M 1982 *Phys. Rev.* B **25** 4925
[27] Tonegawa T and Harada I 1987 *J. Phys. Soc. Japan* **56** 2153
[28] For a review see
Bray J W, Interrante L V, Jacobs I S and Bonner J C 1983 *Extended Linear Chain Compounds* vol 3, ed J S Miller (New York: Plenum) p 353
[29] Hase M, Terasaki I and Uchinokura K 1993 *Phys. Rev. Lett.* **70** 3651
[30] Renard J P, Le Dang K, Veillet P, Dhalenne G, Revcolevschi A and Regnault L P 1995 *Europhys. Lett.* **30** 475
[31] Regnault L P, Renard J P, Dhalenne G and Revcolevschi A 1995 *Europhys. Lett.* **32** 579
[32] Martin M C, Hase M, Hirota K, Shirane G, Sasago Y, Koide N and Uchinokura K 1997 *Phys. Rev.* B **56** 3173
[33] Fukuyama H, Tanimoto T and Saito M 1996 *J. Phys. Soc. Japan* **65** 1182
[34] Dagotto E and Rice T M 1996 *Science* **271** 618
[35] Barnes T, Dagotto E, Riera J and Swanson E S 1993 *Phys. Rev.* B **47** 3196
[36] Gopalan S, Rice T M and Sigrist M 1994 *Phys. Rev.* B **49** 8901
[37] Barnes T and Riera J 1994 *Phys. Rev.* B **50** 6817
[38] Reigrotzki M, Tsunetsugu H and Rice T M 1994 *J. Phys.: Condens. Matter* **6** 9235
[39] Oitmaa J, Singh R R P and Zheng Weihong 1996 *Phys. Rev.* B **54** 1009
[40] White S R, Noack R M and Scalapino D J 1994 *Phys. Rev. Lett.* **73** 886
[41] Chakravarty S, Halperin B I and Nelson D R 1988 *Phys. Rev. Lett.* **60** 1057
Chakravarty S, Halperin B I and Nelson D R 1989 *Phys. Rev.* B **39** 2344
[42] Bednorz J G and Müller K A 1986 *Z. Phys.* B **64** 189

[43] Yildirim T, Harris A B, Aharony A and Wohlman O E 1995 *Phys. Rev.* B **52** 10 239
[44] Kim Y J, Aharony A, Birgeneau R J, Chou F C, Wohlman O E, Erwin R W, Greven M, Harris A B, Kastner M A, Korenblit I Ya, Lee Y S and Shirane G 1999 *Phys. Rev. Lett.* **83** 852
[45] Katsumata K, Hagiwara M, Honda Z, Satooka J, Aharony A, Birgeneau R J, Chou F C, Wohlman O E, Harris A B, Kastner M A, Kim Y J and Lee Y S 2000 *Preprint* cond-mat/0008009
[46] Meyer A, Gleizes A, Girerd J, Verdaguer M and Kahn O 1982 *Inorg. Chem.* **21** 1729
[47] Renard J P, Verdaguer M, Regnault L P, Erkelens W A C, Rossat-Mignod J and Stirling W G 1987 *Europhys. Lett.* **3** 945
[48] Date M and Kindo K 1990 *Phys. Rev. Lett.* **65** 1659
[49] Katsumata K, Hori H, Takeuchi T, Date M, Yamagishi A and Renard J P 1989 *Phys. Rev. Lett.* **63** 86
[50] Botet R, Jullien R and Kolb M 1983 *Phys. Rev.* B **28** 3914
[51] Affleck I 1990 *Phys. Rev.* B **41** 6697
[52] Tsvelik A M 1990 *Phys. Rev.* B **42** 10 499
[53] Golinelli O, Jolicoeur Th and Lacaze R 1993 *J. Phys.: Condens. Matter* **5** 7847
[54] Regnault L P, Zaliznyak I, Renard J P and Vettier C 1994 *Phys. Rev.* B **50** 9174
[55] Lu W, Tuchendler J, von Ortenberg M and Renard J P 1991 *Phys. Rev. Lett.* **67** 3716
[56] Brunel L C, Brill T M, Zaliznyak I, Boucher J P and Renard J P 1992 *Phys. Rev. Lett.* **69** 1699
[57] Sieling M, Palme W and Lüthi B 1995 *Z. Phys.* B **96** 297
[58] Luther S, von Ortenberg M, Tuchendler J and Renard J P 1995 *Physica* B **211** 213
[59] Mitra P P and Halperin B I 1994 *Phys. Rev. Lett.* **72** 912
[60] Sakai T and Shiba H 1994 *J. Phys. Soc. Japan* **63** 867
[61] Chiba M, Ajiro Y, Kikuchi H, Kubo T and Morimoto T 1991 *Phys. Rev.* B **44** 2838
[62] Hagiwara M and Katsumata K 1996 *Phys. Rev.* B **53** 14 319
[63] Avenel O, Xu J, Xia J S, Xu M-F, Andraka B, Lang T, Moyland P L, Ni W, Signore P J C, van Woerkens C M C M, Adams E D, Ihas G G, Meisel M W, Nagler S E, Sullivan N S, Takano Y, Talham D R, Goto T and Fujiwara N 1992 *Phys. Rev.* B **46** 8655
[64] Moses D, Shechter H, Ehrenfreund E and Makovsky J 1977 *J. Phys. C: Solid State Phys.* **10** 433
[65] Sakai T and Takahashi M 1990 *Phys. Rev.* B **42** 4537
[66] Honda Z, Asakawa H and Katsumata K 1998 *Phys. Rev. Lett.* **81** 2566
[67] Honda Z, Katsumata K, Hagiwara M and Tokunaga M 1999 *Phys. Rev.* B **60** 9272
[68] Magariño J, Tuchendler J and Renard J P 1978 *Solid State Commun.* **26** 721
Tuchendler J and Renard J P 1986 *Phys. Rev.* B **33** 620
[69] Osano K, Shiba H and Endoh Y 1982 *Prog. Theor. Phys.* **67** 995
[70] Renard J P, Verdaguer M, Regnault L P, Erkelens W A C, Rossat-Mignod J, Ribas J, Stirling W G and Vettier C 1988 *J. Appl. Phys.* **63** 3538
[71] Kaburagi M and Tonegawa T 1994 *J. Phys. Soc. Japan* **63** 420
[72] Hagiwara M, Katsumata K, Hori H, Takeuchi T, Date M, Yamagishi A, Renard J P and Affleck I 1992 *Physica* B **177** 386
[73] Glarum S H, Geschwind S, Lee K M, Kaplan M L and Michel J 1991 *Phys. Rev. Lett.* **67** 1614
[74] Kimura S, Ohta H, Motokawa M, Yokoo T and Akimitsu J 1998 *J. Phys. Soc. Japan* **67** 2514
[75] Miyashita S and Yamamoto S 1993 *Phys. Rev.* B **48** 913
[76] Hase M, Terasaki I, Uchinokura K, Tokunaga M, Miura N and Obara H 1993 *Phys. Rev.* B **48** 9616
[77] Hamamoto T, Adachi N, Kido G, Hase M, Sasago Y and Uchinokura K 1994 *J. Phys. Soc. Japan* **63** 1218
[78] Harada I and Kotani A 1982 *J. Phys. Soc. Japan* **51** 1737
[79] Buzdin A I, Kulić M L and Tugushev V V 1983 *Solid State Commun.* **48** 483
[80] Fagot-Revurat Y, Horvatić M, Berthier C, Ségransan P, Dhalenne G and Revcolevschi A 1996 *Phys. Rev. Lett.* **77** 1861
[81] Kiryukhin V, Keimer B, Hill J P and Vigliante A 1996 *Phys. Rev. Lett.* **76** 4608
[82] Brill T M, Boucher J P, Voiron J, Dhalenne G, Revcolevschi A and Renard J P 1994 *Phys. Rev. Lett.* **73** 1545
[83] Nojiri H, Ohta H, Okubo S, Fujita O, Akimitsu J and Motokawa M 1999 *J. Phys. Soc. Japan* **68** 3417
[84] Hase M, Hagiwara M and Katsumata K 1996 *Phys. Rev.* B **54** R3722
[85] Nojiri H, Hamamoto T, Wang Z J, Mitsudo S, Motokawa M, Kimura S, Ohta H, Ogiwara S, Fujita O and Akimitsu J 1997 *J. Phys.: Condens. Matter* **9** 1331
[86] Glazkov V N, Smirnov A I, Petrenko O A, Paul D M^{c}K, Vetkin A G and Eremina R M 1998 *J. Phys.: Condens. Matter* **10** 7879
[87] Singh R R P and Gelfand M P 1988 *Phys. Rev. Lett.* **61** 2133
[88] Tonegawa T, Nakao T and Kaburagi M 1996 *J. Phys. Soc. Japan* **65** 3317
[89] Escuer A, Vicente R, Ribas J, El Fallah M S, Solans X and Font-Bardía M 1994 *Inorg. Chem.* **33** 1842

[90] Escuer A, Vicente R, Solans X and Font-Bardía M 1994 *Inorg. Chem.* **33** 6007
[91] Narumi Y, Hagiwara M, Sato R, Kindo K, Nakano H and Takahashi M 1998 *Physica* B **246+247** 509
[92] Narumi Y, Hagiwara M, Kohno M and Kindo K 2000 *Preprint*
[93] Hiroi Z, Azuma M, Takano M and Bando Y 1991 *J. Solid State Chem.* **95** 230
[94] Azuma M, Hiroi Z, Takano M, Ishida K and Kitaoka Y 1994 *Phys. Rev. Lett.* **73** 3463
[95] Matsuda M and Katsumata K 1996 *Phys. Rev.* B **53** 12 201
[96] Matsuda M, Katsumata K, Eisaki H, Motoyama N, Uchida S, Shapiro S M and Shirane G 1996 *Phys. Rev.* B **54** 12 199
[97] Tanaka H, Shiramura W, Takatsu T, Kurniawan B, Takahashi M, Kamishima K, Takizawa K, Mitamura H and Goto T 1998 *Physica* B **246+247** 230
[98] Kurniawan B, Tanaka H, Takatsu K, Shiramura W, Fukuda T, Nojiri H and Motokawa M 1999 *Phys. Rev. Lett.* **82** 1281
[99] Taniguchi S, Nishikawa T, Yasui Y, Kobayashi Y, Sato M, Nishioka T, Kontani M and Sano K 1995 *J. Phys. Soc. Japan* **64** 2758
[100] Kageyama H, Yoshimura K, Stern R, Mushnikov N V, Onizuka K, Kato M, Kosuge K, Slichter C P, Goto T and Ueda Y 1999 *Phys. Rev. Lett.* **82** 3168
[101] Nojiri H, Kageyama H, Onizuka K, Ueda Y and Motokawa M 1999 *J. Phys. Soc. Japan* **68** 2906
[102] For a review see
Mydosh J A 1993 *Spin Glasses: an Experimental Introduction* (London: Taylor and Francis)
[103] For a review on the theoretical developments see
Aharony A 1983 *J. Magn. Magn. Mater.* **31–34** 1432
[104] For a review on the experimental developments see
Katsumata K 1983 *J. Magn. Magn. Mater.* **31–34** 1435
[105] For a review see
Tuchendler J and Katsumata K 1989 *Physica* B **155** 323
[106] See, for example,
Kambe T, Tanaka H, Kimura S, Ohta H, Motokawa M and Nagata K 1996 *J. Phys. Soc. Japan* **65** 1799
[107] For a review see
Gunther L and Barbara B (ed) 1995 *Quantum Tunneling of Magnetization—QTM '94 (NATO ASI Series E, vol 301)* (Dordrecht: Kluwer)
[108] Sessoli R, Tsai H-L, Schake A R, Wang S, Vincent J B, Folting K, Gatteschi D, Christou G and Hendrickson D N 1993 *J. Am. Chem. Soc.* **115** 1804
[109] Barra A L, Gatteschi D and Sessoli R 1997 *Phys. Rev.* B **56** 8192
[110] Hill S, Perenboom J A A J, Dalal N S, Hathaway T, Stalcup T and Brooks J S 1998 *Phys. Rev. Lett.* **80** 2453
[111] Barra A-L, Debrunner P, Gatteschi D, Schulz Ch E and Sessoli R 1996 *Europhys. Lett.* **35** 133